PREDICTING WEB WRINKLES ON ROLLERS

By

J. K. Good, J. A. Beisel, and H. Yurtcu
Oklahoma State University
USA

ABSTRACT

There are two levels of web instability in web lines. The first level of web instability is called web troughs. Web troughs are due to the instability of webs that occur in free web spans. Web troughs have been shown to be predictable using traditional buckling theory. Closed form expressions have been developed and verified in the lab that predict when web troughs will result from roller misalignment and roller taper. Web troughs can be a nuisance in web processes where the web must be planar. The troughs themselves may not damage the web but can be responsible for reductions in web quality after processing that can result in lost profit.

The next level of instability is called web wrinkles. Web wrinkles are due to the instability of webs that are transiting rollers. When webs transit rollers they assume the shape of a sector of a cylindrical shell. A cylindrical shell of web is much more stable than the web in free spans. Compressive stresses which are two to three orders of magnitude larger than those required to induce web troughs are necessary to buckle the cylindrical shell. This paper will demonstrate that web wrinkles are a post buckling phenomena that result from web troughs. The source of the high compressive stresses needed to buckle the web into wrinkles on rollers will be shown. We will show how web wrinkles can be predicted and we will show experimental verification for the cases where a misaligned or tapered rollers were the source of the troughs and wrinkles. Web wrinkles can damage the web as a result of inelastic deformation, fold-overs, and in the worst case may cause full separation or failure of the web. When web wrinkles can be predicted, they can also be prevented.

NOMENCLATURE

a	span length
A_{mn}	amplitude coefficient for buckled shape
A_s	area of a beam which reacts shear, 5bh/6 for a web
b	web width

f_{yi}, f_{yj}	lateral web forces at upstream and downstream rollers, respectively
D	plate bending stiffness, defined in expression (1)
[D]	constitutive matrices relating stress to strain
E	modulus of elasticity
G	shear modulus
h	web thickness
I	web area moment of inertia, $hb^3/12$
m	number of half waves in buckled shape in the x direction
M_i, M_j	web bending moment at upstream and downstream rollers, respectively
n	number of half waves in buckled shape in the y direction
P,Q	constitutive parameters, defined in expression (54)
R	roller radius
T	total web tension, units of force
v_i, v_j	lateral web deflection at upstream and downstream rollers, respectively
w	out of plane web deflection
ε_x,ε_y	x and y direction strains
ε_1, ε_2	principal strains
γ_{xy}	shear strain
ν	Poisson's ratio
ϕ	a shear parameter
σ_e	equivalent stress, defined in expression (3)
σ_{ex}	equivalent stress, defined in expression (25)
σ_x,σ_y	stresses in x and y directions, positive when induces tension
σ_{ycr}	y direction stress required to induce troughs or wrinkles in the web
σ_1, σ_2	principal stresses
θ_i, θ_j	slope of web at upstream and downstream rollers, respectively
θ_{cr}	misalignment or slope of a downstream roller required to induce troughs
τ_{xy}	shear stress in web

INTRODUCTION

Webs undergoing transport can be considered as a series of plate and shell structures as shown in Fig. 1. Webs are often studied as membranes but when investigating instability their small finite bending stiffness must be considered. To successfully transport a web through a machine the web must be subjected to tension. This tension is responsible for forcing the web to conform to the rollers in the shape of a sector of a cylindrical shell. The rollers are supported on low friction bearings on their axes of symmetry. The tension in the web induces normal contact forces between the shells and the surfaces of the rollers. If the tension and friction are sufficient the tangential velocities of the web and the roller surfaces will be essentially equal.

The boundary conditions for webs might appear to depend on the frame of reference of the observer. To a first observer traveling with the web it would appear to be a moving boundary condition problem as plates become cylindrical shells and shells become plates. To a second observer standing to the side of a process machine the plates and shells appear to be of fixed dimensions and have steady state boundary conditions, even though the web is moving through the machine. The dynamic forces associated with moving boundary conditions are typically small for webs due to little mass and for the discussion herein will be assumed negligible. With this in mind the boundary conditions will be

defined in the frame of reference of the second observer. The plates are supported at two opposing ends by rollers. The two remaining edges of each plate appear unsupported. The shells are given contact support by the roller surfaces but this support will not prevent buckling instability of the shell.

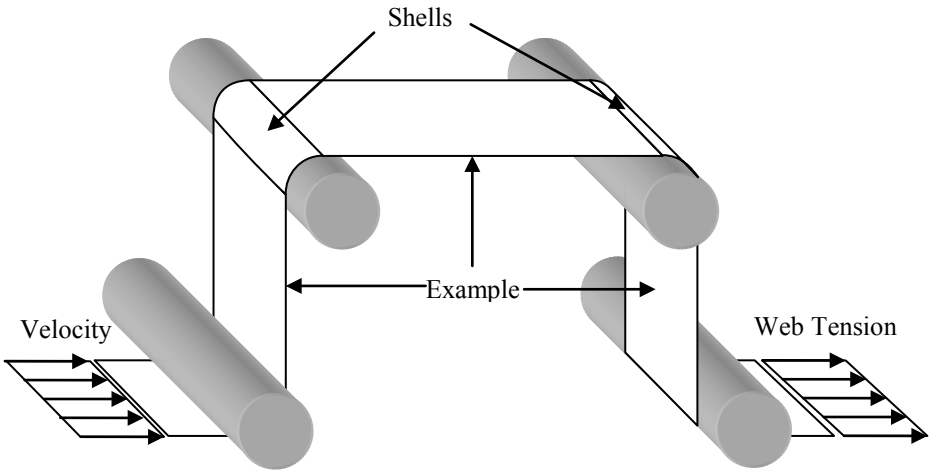

Figure 1 – A Web in Transport through a Process Machine

When discussing the stability of a web, one or more behaviors may exist. The first and most desirable behavior would be a stable web. In this case there would be no out-of-plane deformation of the plates and the shells would have the shape of perfect cylindrical sectors. The second behavior is described as troughs. Troughs are out-of-plane deformations of the web plates. Web troughs may or may not be acceptable in sections of a process machine depending on whether a process is taking place that requires the web to be flat. The third behavior is called wrinkling. Wrinkling is defined as the instability of the web shells. Wrinkling is rarely acceptable under any circumstances as the result is either inelastic deformation of the web or fracture of the web which interrupts the process. Experiments which will be discussed herein have shown that wrinkling of the web shells on rollers is always precipitated by troughs in the free spans (i.e. the plates of web between rollers). It will be shown that troughs can be predicted by linear plate buckling theory. It will also be shown that to predict wrinkling requires the use of nonlinear post-buckling analysis. These analyses are required to determine what compressive stresses are induced in the webs shells by the free spans of web which have already buckled into troughs.

WEB TROUGH FAILURE THEORY

Web Troughs in Isotropic Web

Web troughs are due to instabilities of the web plates between rollers. It may be assumed that the web was initially stable but due to compressive stresses in the y direction that troughs have resulted. An isotropic plate of web, having a width b, spans the distance a between two rollers as shown in Fig. 2.

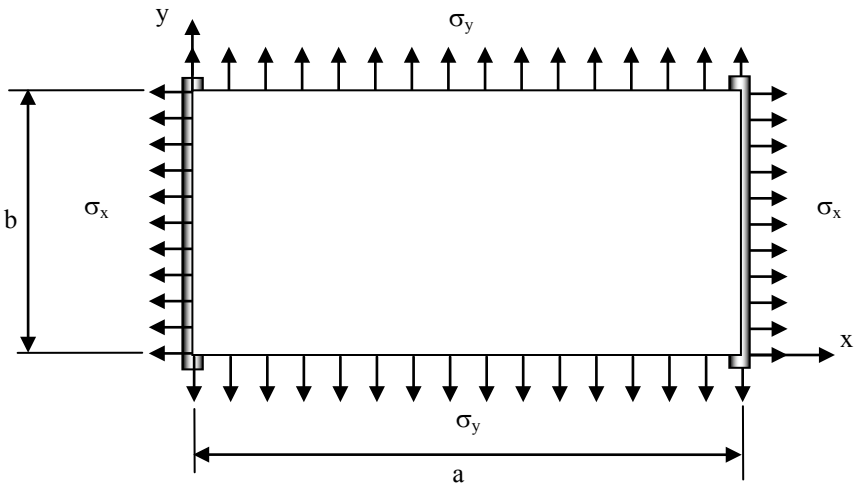

Figure 2 – Isotropic Span of Web between Rollers

The deflection equation for an isotropic plate of thickness *h,* including the effects of membrane forces, is [1]:

$$D\frac{\partial^4 w}{\partial x^4}+2D\frac{\partial^4 w}{\partial x^2\partial y^2}+D\frac{\partial^4 w}{\partial y^4}-\sigma_x h\frac{\partial^2 w}{\partial x^2}-\sigma_y h\frac{\partial^2 w}{\partial y^2}=0 \text{ where } D=\frac{Eh^3}{12\left(1-\nu^2\right)} \qquad \{1\}$$

A solution is sought for the out-of-plane deformation w (in the z direction) of the form:

$$w = A_{mn}\sin\left(\frac{m\pi x}{a}\right)\sin\left(\frac{n\pi y}{b}\right) \qquad \{2\}$$

where *m* and *n* are the half wave numbers in the *x* and *y* directions, respectively and A_{mn} is the maximum amplitude of out-of-plane deformation for a given buckled shape. It should be noted that by selecting the displacement form {2}, the out-of-plane deformation is forced to vanish on all four boundaries of the web span when *m* and *n* are forced to be positive integers. While this appears appropriate on the boundaries that contact the rollers, no such kinematic constraint exists on the free web boundaries (y=0,b). Observations of troughs in the laboratory demonstrate that the free edge deformations appear negligible compared to the out-of-plane deformations associated with the troughs. From surface equilibrium no σ_y stress can exist at the free boundaries and thus troughs would be expected to dissipate near those boundaries which agree with observations. The combination of the absence of troughs and that web tension acts to restrict the out-of-plane deformation *w* supports the assignment of the simple support boundary condition to these boundaries (y=0,b). The moments at the boundaries are related to the second derivative of the deformation *w* which per expression {2} will vanish on the boundaries as long as *m* and *n* are defined as positive integers. Thus the selection of a simple support at these boundaries (y=0,b) is most appropriate. The validity of the assumed form of deformation will be verified later herein by test.

In this analysis it will be assumed that the σ_x stress is positive and thus tensile which restricts the half wave number in the x direction (m) to be unity. If expression {2} is substituted into expression {1} and if that expression is solved for σ_y a relationship for the critical buckling stress is produced of the form:

$$\sigma_{ycr} = -\frac{\left(b^2+a^2n^2\right)^2\sigma_e + b^4\sigma_x}{a^2b^2n^2} \quad \text{where } \sigma_e = \frac{\pi^2 D}{a^2 h} \qquad \{3\}$$

With this expression for a plate of given dimensions and material the critical compressive stress in the *y* direction can be determined as a function of the half wave number in the *y* direction (n) and the tensile stress in the *x* direction (σ_x). Increasing the values of these parameters both serve to increase the magnitude of σ_{ycr} and thus stabilize the web. To determine the value of *n* which is correct for a given value of σ_x requires consideration of minimum energy. For given values of *a*, *b* and *n*, note expression {3} is a linear relationship between σ_{ycr} and σ_x. In Fig. 3, expression {3} has been plotted for the case of a square web (b=a) and fixed positive integer values of *n*. Note that non-integer values of *n* would appear to violate the boundary conditions for the deformation (w) at the boundaries of the web. Also, note the intersection of the *n*=3 and *n*=4 lines that occurs when $\sigma_x=143\sigma_e$. The *n*=3 line should be used as the critical relation for the *y* stress for tensions less than the intersection point while the *n*=4 line should be used when the tension is greater than the intersection point. For a given value of tension (σ_x) the failure criterion will be the line that has the smaller magnitude of σ_{ycr}, hence resulting in the minimum energy. If it is assumed momentarily that *n* is continuous, the energy can be minimized by taking the derivative of {3} with respect to *n*, setting the result to zero and solving for *n*:

$$n = \frac{b}{a}\left(1+\frac{\sigma_x}{\sigma_e}\right)^{1/4} \qquad \{4\}$$

When expression {4} is substituted into {3} an expression is obtained for the critical stress that will cause troughs to occur in an isotropic web:

$$\sigma_{ycr} = -2\left(\sigma_e + \sqrt{\sigma_e^2 + \sigma_e\sigma_x}\right) \qquad \{5\}$$

Substitution of typical web values for h, a, σ_x, E, and ν into this expression demonstrates that the σ_e term is 4 orders of magnitude smaller than σ_x. Thus expression {5} simplifies to:

$$\sigma_{ycr} \approx -2\sqrt{\sigma_e\sigma_x} = -\frac{\pi h}{a}\sqrt{\frac{E\sigma_x}{3\left(1-\nu^2\right)}} \qquad \{6\}$$

Note that web tension which induces the σ_x stress in the web acts to stabilize the web (i.e. the more σ_x stress is applied allows the web to accept a more negative σ_y stress prior to producing troughs). The wavelength of these troughs will be:

$$\lambda = \frac{b}{n/2} = \frac{2a}{\left(1+\frac{\sigma_x}{\sigma_e}\right)^{1/4}} \qquad \{7\}$$

Expression {5} is also shown in Fig. 3 and agrees with the piecewise linear solutions nicely, note the greatest disagreement is in the vicinity of the intersections. Expressions {6} and {7} are valid for web spans with various *a* and *b* dimensions but note the expressions are only dependent on the span length *a*.

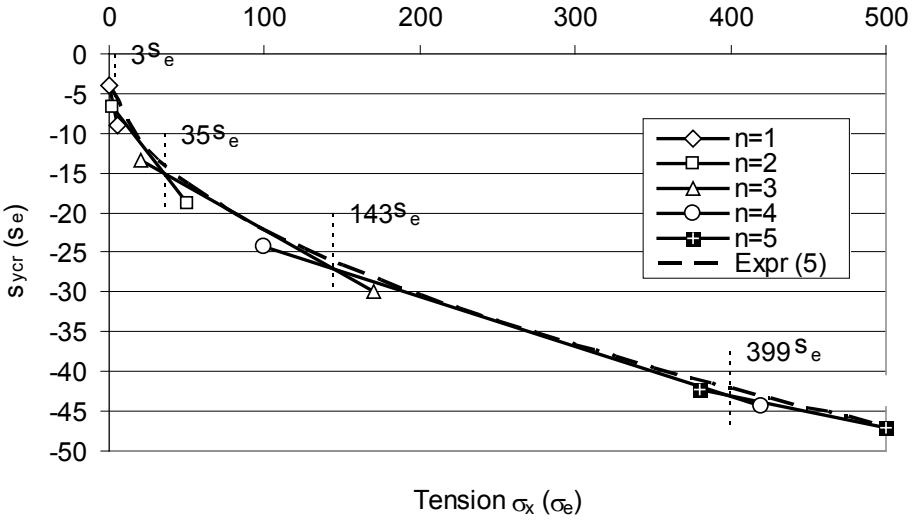

Figure 3 – Instability of Isotropic web Panels (*b=a*).

In applying expression {6} it will be noted that very little *y* direction compressive stress may be needed to induce instability. When the σ_y stresses become more negative than the critical buckling stress from expression {6} the web has buckled and developed troughs, thus tension field behavior has begun.

Web Troughs in Orthotropic Webs

The deflection equation for an orthotropic plate including the effects of membrane forces is [2]:

$$D_1\frac{\partial^4 w}{\partial x^4} + 2D_3\frac{\partial^4 w}{\partial x^2\partial y^2} + D_2\frac{\partial^4 w}{\partial y^4} - \sigma_x h\frac{\partial^2 w}{\partial x^2} - \sigma_y h\frac{\partial^2 w}{\partial y^2} = 0 \qquad \{8\}$$

where:

$$D_1 = \frac{E_x h^3}{12\left(1-\nu_{xy}\nu_{yx}\right)} \quad D_2 = \frac{E_y h^3}{12\left(1-\nu_{xy}\nu_{yx}\right)} \quad D_3 = D_1\nu_{xy} + 2D_k \quad D_k = \frac{Gh^3}{12} \qquad \{9\}$$

and E_x and E_y are the moduli of elasticity in the x and y directions and G is the shear modulus. The Poisson's ratios are perhaps best defined by the constitutive relations between strain (ε) and stress (σ) in the x and y directions:

$$\varepsilon_x = \frac{\sigma_x}{E_x} - \frac{\nu_{yx}\sigma_y}{E_y} \quad \varepsilon_y = \frac{\sigma_y}{E_y} - \frac{\nu_{xy}\sigma_x}{E_x} \quad \gamma_{xy} = \frac{1}{G}\tau_{xy} \qquad \{10\}$$

If expression {2} is substituted into expression {8} using m=1:

$$\sigma_{eo}\left[\sqrt{\frac{D_1}{D_2}} + 2\left(\frac{an}{b}\right)^2 \frac{D_3}{\sqrt{D_1 D_2}} + \left(\frac{an}{b}\right)^4 \sqrt{\frac{D_2}{D_1}}\right] + \sigma_x + \left(\frac{an}{b}\right)^2 \sigma_y = 0 \qquad \{11\}$$

where $\sigma_{eo} = \frac{\pi^2\sqrt{D_1 D_2}}{a^2 h}$. Solving this expression for the σ_y stress yields:

$$\sigma_y = -\left\{\sigma_{eo}\left[\sqrt{\frac{D_1}{D_2}} + 2\left(\frac{an}{b}\right)^2 \frac{D_3}{\sqrt{D_1 D_2}} + \left(\frac{an}{b}\right)^4 \sqrt{\frac{D_2}{D_1}}\right] + \sigma_x\right\}\left(\frac{b}{an}\right)^2 \qquad \{12\}$$

Similar to the derivation for the isotropic web it is assumed momentarily that *n* is continuous, that the strain energy will be minimized by taking the derivative of {12} with respect to *n*, setting the result to zero and solving for *n*:

$$n = \frac{b}{a\sqrt{\pi}} \sqrt[4]{\frac{\pi^2 D_1 + ha^2\sigma_x}{D_2}} = \frac{b}{a}\left(\frac{D_1}{D_2} + \frac{ha^2\sigma_x}{\pi^2 D_2}\right)^{\frac{1}{4}} \qquad \{13\}$$

Note if D_2 approaches D_1 that expression {13} simplifies to the isotropic form {4}. The wavelength of the troughs in an orthotropic web will be:

$$\lambda = \frac{b}{n/2} = \frac{2a}{\left(\frac{D_1}{D_2} + \frac{ha^2\sigma_x}{\pi^2 D_2}\right)^{1/4}} \qquad \{14\}$$

Substituting expression {13} into the expression for σ_y {12} yields the buckling stress σ_{ycr} for an orthotropic web:

$$\sigma_{ycr} = -\frac{2\pi}{a^2 h} \frac{\left(\pi^2 D_1\sqrt{D_2} + ha^2\sigma_x\sqrt{D_2} + \pi D_3\sqrt{\pi^2 D_1 + ha^2\sigma_x}\right)}{\sqrt{\pi^2 D_1 + ha^2\sigma_x}} \qquad \{15\}$$

Substitution of typical web values for h, a, σ_x, E_x, ν_{xy}, and ν_{yx} into our expression for n shows the $\pi^2 D_1$ term is three to four orders of magnitude smaller than the $ha^2\sigma_x$ term. This simplifies the half wave number to:

$$n \approx \frac{b}{a\sqrt{\pi}}\left(\frac{ha^2\sigma_x}{D_2}\right)^{\frac{1}{4}} = b\sqrt{\frac{2}{\pi ah}}\left(\frac{3\left(1-\nu_{xy}\nu_{yx}\right)\sigma_x}{E_y}\right)^{\frac{1}{4}} \quad \{16\}$$

This also allows a simplification of the critical buckling stress:

$$\sigma_{ycr} \approx -\frac{\pi h}{a}\sqrt{\frac{\sigma_x E_y}{3\left(1-\nu_{xy}\nu_{yx}\right)}} \quad \{17\}$$

Note the similarity between expression {17} for the orthotropic web and expression {6} for the isotropic web. It appears that the greatest impact of orthotropic web properties is that the modulus in the cross machine direction E_y must be used in the instability calculations.

DISTURBANCES WHICH INDUCE WEB TROUGHS

For the web between rollers to become unstable and produce troughs, negative σ_y stresses comparable to those given in expressions {6} and {17} must be applied. Disturbances which are common in web lines include misaligned rollers and rollers that may have unintentional taper in diameter. How these disturbances induce negative σ_y stresses in the web will now be examined.

Webs in Spans with Misaligned Rollers

A common problem in web process lines is the steering of webs by misaligned rollers. If a roller that is initially parallel to an upstream roller is slowly misaligned the web will be steered laterally an amount v_j for a misalignment θ_j as shown in Fig. 4. As the misalignment is further increased a critical value will be reached and troughs will appear. If the misalignment is increased yet further a second critical value will be surpassed and wrinkles will be induced into the web material on the rollers.

The material upstream of the misaligned roller behaves similarly to an end loaded cantilever beam provided that friction forces are sufficient to enforce the boundary conditions. Shelton discussed the concept of normal entry and exit conditions of webs entering and leaving rollers [3]. Webs approach or enter rollers normal to axis of rotation of that roller. A misaligned roller has a misaligned axis of rotation and the web will enter that roller normally to that misaligned axis, refer to Fig. 4. The analogy to the end loaded cantilever is that the moment in this span increases linearly from zero at the misaligned roller to a maximum value at the upstream roller. Thus the σ_x in the web just upstream of the misaligned web is uniform while at the upstream roller a linear variation in σ_x stress associated with the maximum moment exists. Shelton was first to deduce this.

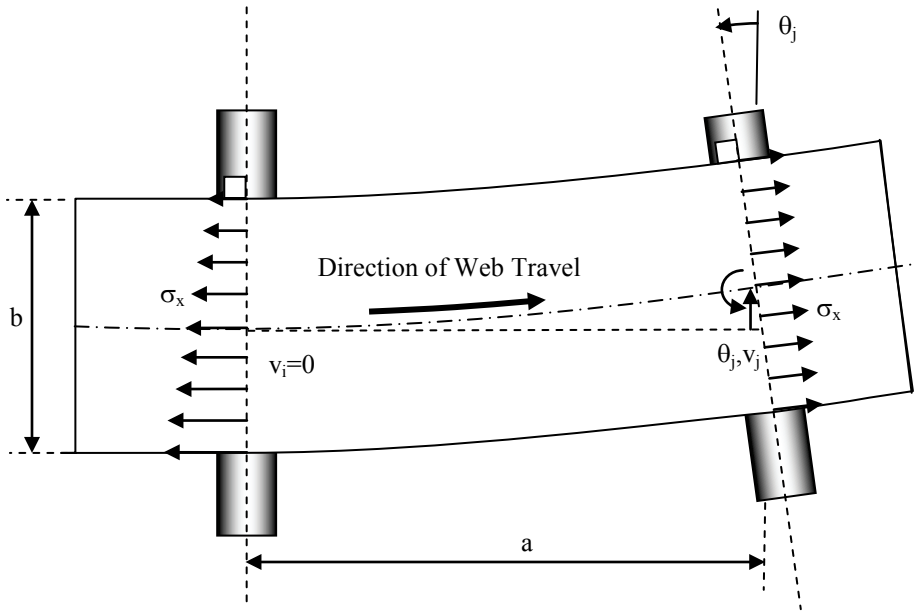

Figure 4 – A web span between rollers i and j

Przemieniecki developed stiffness matrices for beams stiffened by tension and shear effects [4]. The stiffness matrix for this beam is:

$$\begin{Bmatrix} f_{yi} \\ M_i \\ f_{yj} \\ M_j \end{Bmatrix} = \begin{bmatrix} \frac{12EI}{a^3(1+\phi)}+\frac{6T}{5a} & \frac{6EI}{a^2(1+\phi)}+\frac{T}{10} & -\frac{12EI}{a^3(1+\phi)}-\frac{6T}{5a} & \frac{6EI}{a^2(1+\phi)}+\frac{T}{10} \\ \frac{6EI}{a^2(1+\phi)}+\frac{T}{10} & \frac{(4+\phi)EI}{a(1+\phi)}+\frac{2Ta}{15} & -\frac{6EI}{a^2(1+\phi)}-\frac{T}{10} & \frac{(2-\phi)EI}{a(1+\phi)}-\frac{Ta}{30} \\ -\frac{12EI}{a^3(1+\phi)}-\frac{6T}{5a} & -\frac{6EI}{a^2(1+\phi)}-\frac{T}{10} & \frac{12EI}{a^3(1+\phi)}+\frac{6T}{5a} & -\frac{6EI}{a^2(1+\phi)}-\frac{T}{10} \\ \frac{6EI}{a^2(1+\phi)}+\frac{T}{10} & \frac{(2-\phi)EI}{a(1+\phi)}-\frac{Ta}{30} & -\frac{6EI}{a^2(1+\phi)}-\frac{T}{10} & \frac{(4+\phi)EI}{a(1+\phi)}+\frac{2Ta}{15} \end{bmatrix} \begin{Bmatrix} v_i \\ \theta_i \\ v_j \\ \theta_j \end{Bmatrix} \quad \{18\}$$

where ϕ is defined as the shear parameter:

$$\phi = \frac{12EI}{GA_s a^2} \quad \{19\}$$

and A_s is the area of the cross section subject to shear. For the rectangular cross section of a web the area subject to shear is: $A_s=5bh/6$. It is assumed the web is a beam and that it is supported by rollers at i and j in Fig. 4 and that the web is traveling from left to right and that the roller at position j is misaligned to some degree θ_j. This will induce a shear force and therefore some lateral deformation v into the span. At the upstream roller it will be arbitrarily assumed that v_i is zero without loss of generality. The rotation at i will be non-zero due to the shear deformation and equal to:

$$\theta_i = \frac{f_{yj}}{GA_s} \qquad \{20\}$$

Shelton determined that the moment in the web just prior to a downstream roller is zero under steady-state conditions [3]. Thus with knowledge that M_j is zero the fourth equation in the stiffness matrix {18} can be solved for v_j as:

$$v_j = \frac{a\left[Ta^2\left(4A_sG\theta_j - f_{yj}\right)(1+\phi) + 30EI\left[f_{yj}(2-\phi) + A_sG\theta_j(4+\phi)\right]\right]}{3A_sG\left[60EI + Ta^2(1+\phi)\right]} \qquad \{21\}$$

With v_i assumed zero and θ_i and v_j known, the third expression in the stiffness matrix {18} yields an expression relating f_{yj}, and thereby the shear in the web F, to the misalignment of the downstream roller θ_j:

$$f_{yj} = F = \frac{A_sG\left[240E^2I^2 + 3T^2a^4(1+\phi) + 8EITa^2(13+3\phi)\right]}{240E^2I^2 + Ta^4(2A_sG+T)(1+\phi) + 8EIa^2\left[15A_sG - T(2-3\phi)\right]}\theta_j \qquad \{22\}$$

This expression has bounds of validity that include limiting the downstream roller misalignment θ_j to values that will prevent web edge slackness at the upstream roller and the assumption that the lateral force f_{yj} does not exceed the force which can be sustained by friction between the web and roller.

Expression {22} can be used to determine the shear stress τ_{xy} in the web. The average shear stress was determined by dividing the shear by the cross section area. The second principal stress will be negative (compressive) and can be determined using the expression:

$$\sigma_2 = \frac{\sigma_x}{2} - \sqrt{\left(\frac{\sigma_x}{2}\right)^2 + {\tau_{xy}}^2} \qquad \{23\}$$

If this principal stress is equated to the critical stress from expression {17} the critical rotation to induce troughs in the web can be determined:

$$\theta_{cr,\tau_{avg}} = \frac{6\left(5b^6E^2h^2 + a^4T(5bGh+3T)(1+\phi) + a^2b^3Eh\left(25bGh + T(6\phi-4)\right)\right)}{5G\left(5b^6E^2h^2 + 9a^4T^2(1+\phi) + 2a^2b^3EhT(13+3\phi)\right)}\sigma_{ex} \qquad \{24\}$$

where:

$$\sigma_{ex} = \sqrt{\sigma_{ycr}\left(\sigma_{ycr} - \frac{T}{bh}\right)} \qquad \{25\}$$

and where σ_{ycr} can be substituted from the isotropic expression {6} or the orthotropic expression {17}. At this rotation of the downstream roller troughs would be expected across much of the web width. Troughs should first appear at the center of the web where the flexural shear stress is maximum, 1.5 times greater than the average value. If the

maximum shear stress is inserted into expression {23}, the principal stress can again be equated to the critical buckling stress to provide an expression for the critical rotation to predict the onset of troughs:

$$\theta_{cr,\tau_{max}} = \frac{4\left(5b^6E^2h^2 + a^4T(5bGh+3T)(1+\phi) + a^2b^3Eh\left(25bGh + T(6\phi-4)\right)\right)}{5G\left(5b^6E^2h^2 + 9a^4T^2(1+\phi) + 2a^2b^3EhT(13+3\phi)\right)}\sigma_{ex} \quad \{26\}$$

The second principal stress in expression {23} is nearly but not quite aligned with the y direction. The amount α that the principal stress is misaligned from the y axis can be determined from the expression $\tan(2\alpha) = \frac{2\tau}{\sigma_x}$. The values of shear stress τ required to buckle a web are often two to three orders of magnitude less than the machine direction stress, thus the misalignment α is negligible. Equating the principal stress in expression {23} with the critical buckling stress is not exact and is an assumption whose legitimacy will be proven in the verification tests. As stated earlier a misaligned roller causes the web to behave as an end loaded cantilever beam. The σ_x stress will be a bending term which will vary linearly with *x* and *y* plus a constant term due to web tension. Expressions {6} and {17} were developed for constant values of σ_x and σ_y throughout the domain of the plate. Also note that expression {6} and {17}) are dependent on the span length *a* but independent of the web width *b*. Thus expressions {6} and {17} are applicable to sub widths of the original span, perhaps as narrow as *b/n*.

To demonstrate the efficacy of expressions {24} and {26} a test was setup with an isotropic polyester web, an orthotropic newsprint web and an orthotropic spunbond nonwoven web. The properties for these webs are given in Table 1.

Web Material	h (μm)	b (cm)	E_x (MPa)	E_y (MPa)	ν_{xy}	ν_{yx}	G (MPa)
polyester film	23.4	15.24	5000	5000	.3	.3	1920
newsprint	71	15.7	4340	2760	.3	.19	1430
polypropylene non-woven	127	10.6	55.1	8.27	.3	.04	6.67

Table 1 – Web Material Properties used in Verification Tests

The experimental setup is shown in Fig. 5. In these tests the polyester web would travel from left to right. The web was subjected to constant tension that was measured just upstream of the test section. The roller at the right is supported by a yoke and the alignment of the yoke θ_j is precisely controlled with an end micrometer. The nominal radii of the rollers are all 3.68 cm (1.45 in). The yoke sits atop a mechanical slide such that the span length *a* was easily manipulated. At the beginning of a test the axis of rotation of the downstream roller could begin aligned with the axis of rotation of the upstream roller and the web would pass through this section completely planar with no

indication of instability. Then the yoke and thus the axis of rotation of the downstream roller was slowly misaligned until troughs appeared as shown in Fig. 5. The angular misalignment θ_j at which the troughs appeared was then recorded. Then the misalignment would be increased further until a wrinkle formed in the web on the misaligned roller and that misalignment was recorded as well.

In Figs. 6, 7, and 8 the test results are compared to the model results. Expressions {24} and {26} both capture the trends of the data quite nicely. Expression {24} which was developed using an assumption of an average shear stress distribution provides the best estimation of the test results.

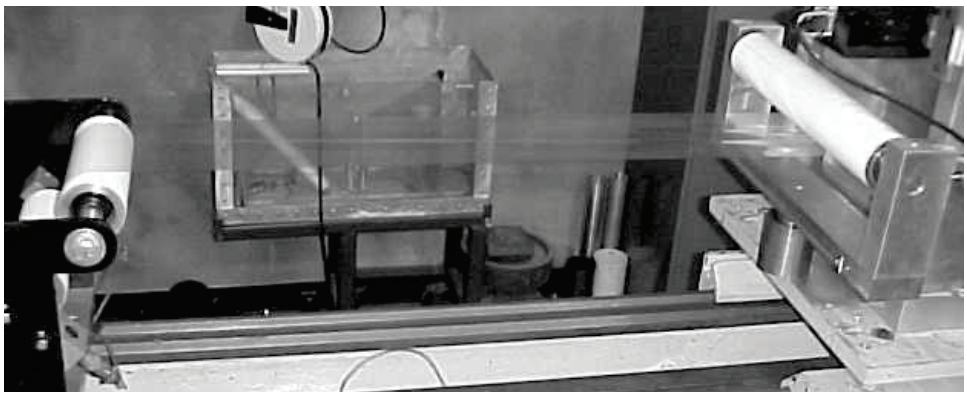

Figure 5 – Experimental Setup for Testing the Roller Misalignment needed to Induce Troughs and Wrinkles

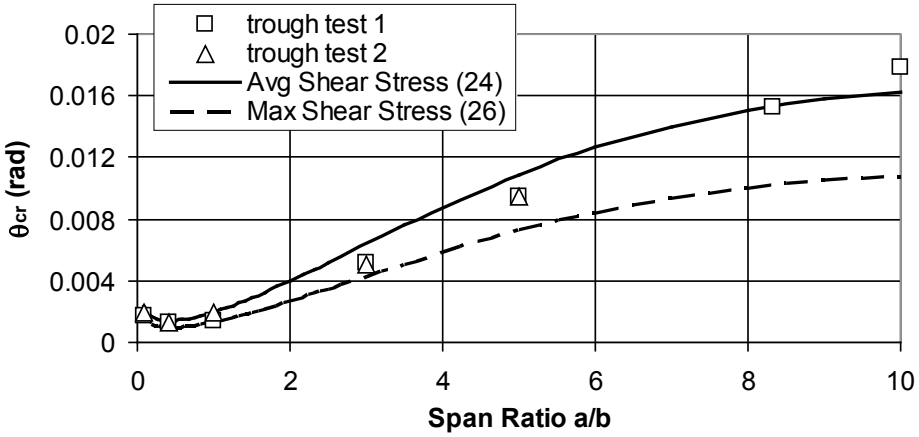

Figure 6 – Predicted and Tested Misalignments required to Produce Troughs in a Polyester Web when the web tension T was 54.7 N (12.3 lbs)

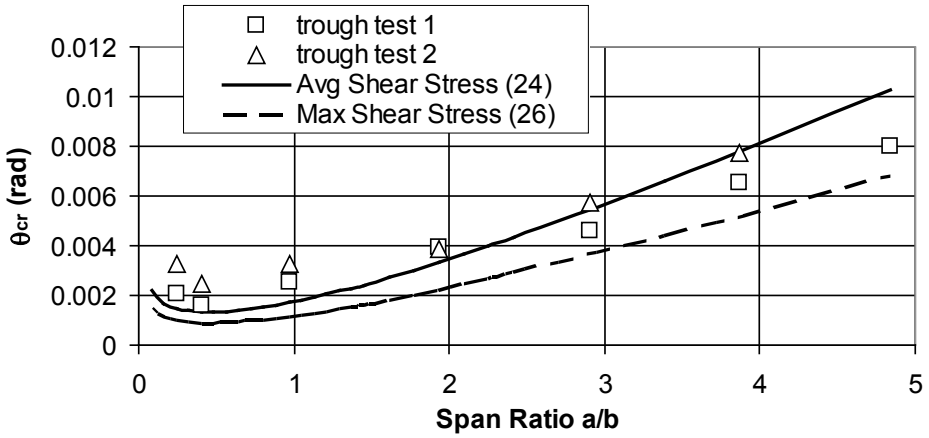

Figure 7 – Predicted and Tested Misalignments required to Produce Troughs in a Newsprint Web when the web tension T was 66.7 N (15 lbs)

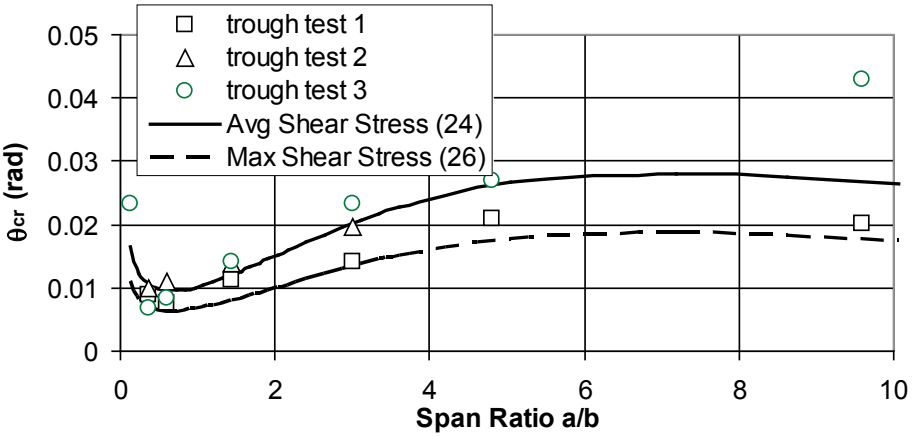

Figure 8 – Predicted and Tested Misalignments required to Produce Troughs in a Nonwoven Web when the web tension T was 6.67 N (1.5 lbs)

Webs in Spans with a Downstream Tapered Roller

Diametral taper of rollers is a common occurrence resulting from the manufacturing processes for rollers. Only minor amounts of taper are needed to induce troughs in webs. A web approaching a tapered roller will still follow the normal entry rule. In Figure 9 a diagram of a tapered roller is shown with the taper somewhat over emphasized such that it can be seen.

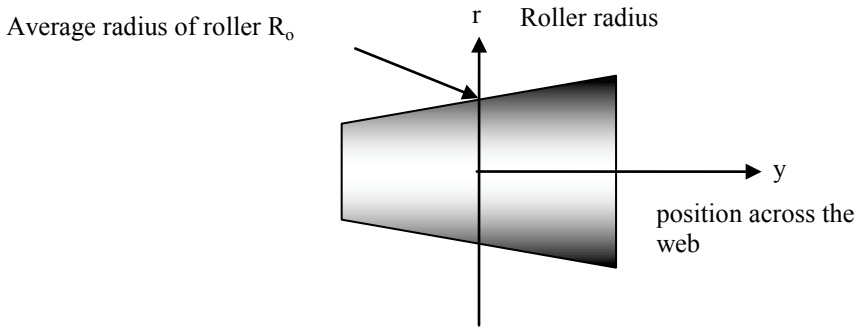

Figure 9 – A Tapered Roller

The origin of the y coordinate is at the lateral center of the roller and would have been the location of the center of the web had the roller not been tapered. The tapered roller can have but one angular velocity (ω) but the surface velocity of the roller will vary with the roller radius. A linear taper will be assumed in this case such the roller radius can be described as:

$$r(y) = my + R_o \qquad \{27\}$$

The velocity across the roller width and the average velocity are:

$$V(y) = r(y)\omega = (my + R_o)\omega \qquad V_{avg} = R_o\omega \qquad \{28\}$$

Assuming no slippage this variation in velocity across the web width will induce a strain and a stress into the web:

$$\varepsilon_{md}(y) = \frac{V(y) - V_{avg}}{V_{avg}} = \frac{my}{R_o} \qquad \sigma(y) = E\varepsilon_{md}(y) = \frac{Emy}{R_o} \qquad \{29\}$$

The variation in stress across the web width induces a steering moment on the web:

$$M_j = \int_{\frac{-b}{2}}^{\frac{b}{2}} -\sigma(y)hydy = \int_{\frac{-b}{2}}^{\frac{b}{2}} \frac{-Emhy^2}{R_o}dy = \frac{-mEhb^3}{12R_o} \qquad \{30\}$$

This moment will steer the web toward the edge of the tapered roller that has the highest diameter as shown in Figure 10.

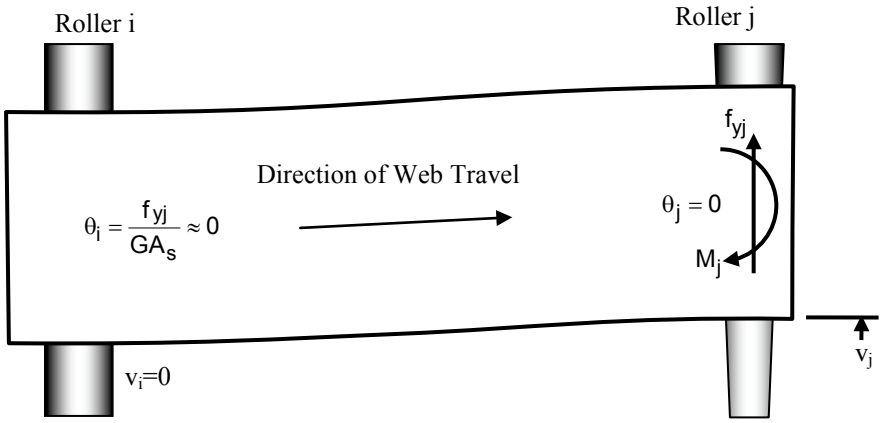

Figure 10 – A Web encountering a Tapered Roller

After applying the boundary conditions for v_i, θ_i, θ_j and the moment M_j {30} to the stiffness matrix presented earlier {18} the 3rd and 4th rows can be solved for f_{yj} and then set equal to one another. The result can be solved for the web deflection at the downstream roller v_j:

$$v_j = \frac{mhb^3E_x}{6R_o} \cdot \frac{-60E_xI + (5GA_sa^2 - Ta^2)(1+\phi)}{[60E_xI + Ta^2(1+\phi)](T + GA_s)} \qquad \{31\}$$

The shear force f_{yj} can be determined by solving the 3rd and 4th rows of the stiffness matrix can be solved for the lateral deformation v_j and then set equal to one another. The result can be solved for the lateral force in the web at the downstream roller which is also the shear force in the web:

$$f_{yj} = \frac{mhb^3E_x}{R_oa} \frac{GA_s[10E_xI + T \cdot a^2(1+\phi)]}{[60E_xI + Ta^2(1+\phi)](T + GA_s)} \qquad \{32\}$$

This shear force f_{yj} can now be used to form the maximum shear stress in the principal stress relation set equal to the critical buckling stress from expressions {6} or {17}:

$$\sigma_2 = \sigma_{ycr} = \frac{\sigma_x}{2} - \sqrt{\left(\frac{\sigma_x}{2}\right)^2 + \tau_{xy}{}^2} = \frac{T}{2bh} - \sqrt{\left(\frac{T}{2bh}\right)^2 + \left(\frac{3f_{yj}}{2bh}\right)^2} \qquad \{33\}$$

If f_{yj} is input to expression {33}, the result can be solved for *m* which is the critical taper that will cause troughs to form in the web:

$$m_{cr} = \frac{2aR_o}{3b^2E_x} \frac{\left[60E_xI + Ta^2(1+\phi)\right](T + GA_s)}{GA_s\left[10E_xI + Ta^2(1+\phi)\right]}\sigma_{ex} \qquad \{34\}$$

where σ_{ex} is found in expression {25} and I is the area moment of inertia of the web ($hb^3/12$).

To demonstrate the efficacy of expression {34} a test was setup with an isotropic polyester web. The properties of this web were given in Table 1. The experimental setup is shown in Fig. 11. To conduct these tests several rollers were machined with intentional taper with a nominal radius of 3.68 cm (1.45 in.). Web tension has a stabilizing influence on the trough buckling stress as was shown in expressions {6} and {17}. In these tests web tension would be set high and then slowly reduced until troughs appeared.

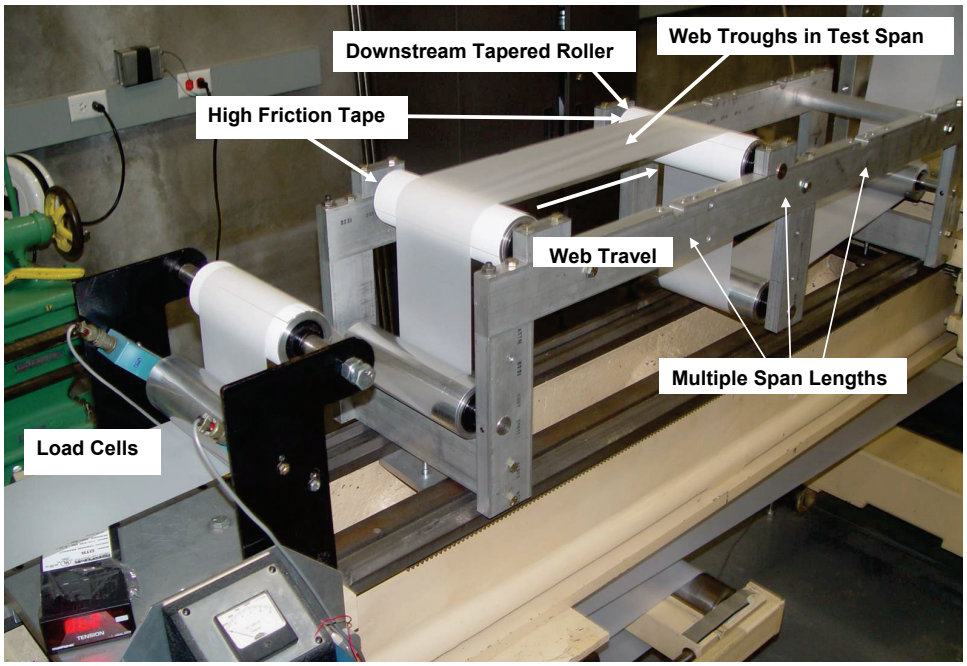

Figure 11 – Experimental Setup for Testing the Roller Taper needed to Induce Troughs and Wrinkles

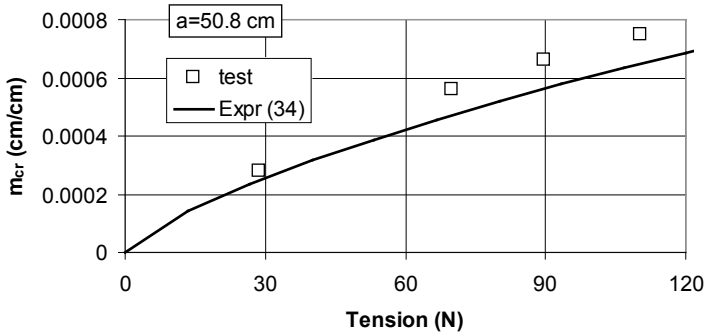

Figure 12 – Critical Roller Taper Required to Trough a Polyester Web in a Web Span 50.8 cm in Length

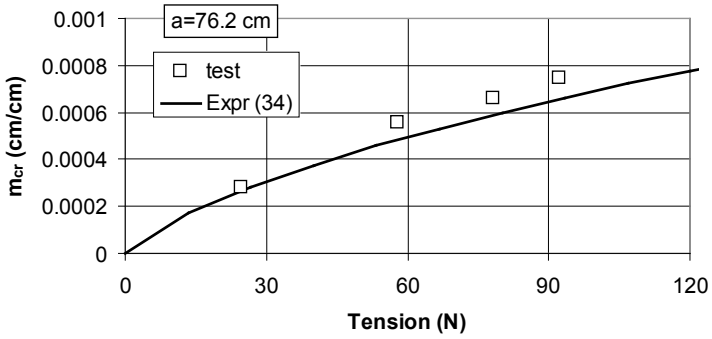

Figure 13 – Critical Roller Taper Required to Trough a Polyester Web in a Web Span 76.2 cm in Length

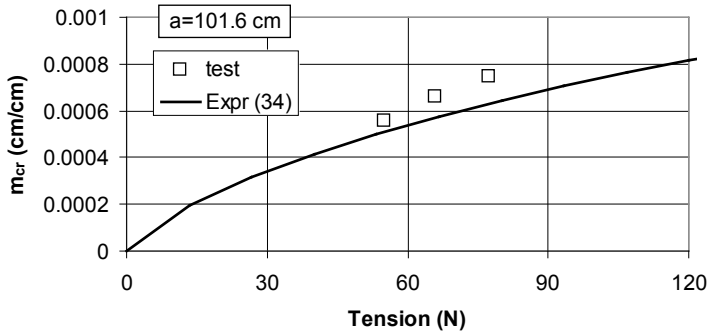

Figure 14 – Critical Roller Taper Required to Trough a Polyester Web in a Web Span 101.6 cm in Length

WEB WRINKLE FAILURE THEORY

Much larger compressive stresses are required to buckle the shells that separate the flat web sections. As web tension increases, the width of the flat web sections becomes less than *b* due to Poisson contraction. After the flat web sections have developed troughs their projected width reduces even further. As a web with troughs approaches a roller the amplitude of the troughs dissipate per expression {2} and the deformed web width must become compatible to the width of the web on the rollers, also less than *b* but due only to web tension and Poisson contraction. Thus the web shells will assume some compressive stress, the levels of which will be discussed later.

Shell Buckling of Isotropic Webs

The axial buckling stress of cylindrical shells or sectors thereof of radius *R* was historically a topic of perplexity in the field of mechanics. Timoshenko developed the failure algorithm [5]:

$$\sigma_{ycr} = -\frac{Eh}{R\sqrt{3\left(1-\nu^2\right)}} \qquad \{35\}$$

The confusion was that extensive testing of metal cylindrical shells supported the conclusion that these shells truly buckled at stresses ranging from 15 to 60% of the theoretical value {35} depending on R/h. It was concluded that small imperfections in the tested shells and the end constraints were responsible for the reduction. This was later shown by Weingarten[6] who proved that expression {35} was accurate for cylindrical shells composed of polyester film that were internally stabilized by pressure. The webs that wrap rollers simulate sectors of cylindrical shells that are internally pressurized. The internal pressure is due to web tension and can be predicted using the hoop stress expression for a thin wall pressure vessel (P=□x h/R). Expression {18} has proven to be accurate for predicting the buckling stress of web shells as will be shown later.

SHELL BUCKLING OF ORTHOTROPIC WEBS

In Figure 15 an element of a thin orthotropic cylindrical shell is shown.

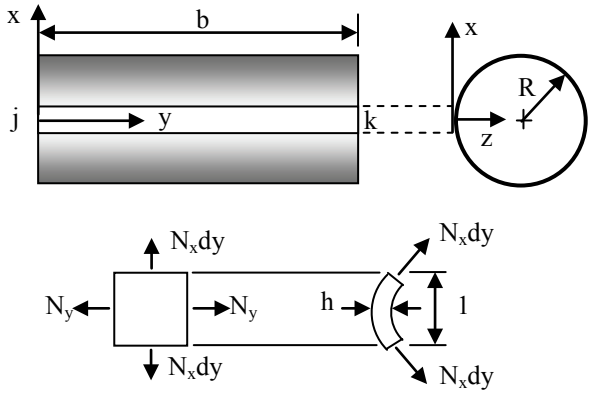

Figure 15 – Nomenclature for the Instability of a Cylinder

The constitutive expressions in expression {10} can be written in terms of stresses and if multiplied by the shell thickness *h* will yield expressions relating the membrane forces to the strains. When an axisymmetric structure is subject to axisymmetric loading the circumferential strain ε_x becomes –w/R and thus the membrane forces can be written:

$$N_x = \frac{E_x h}{1-\nu_{xy}\nu_{yx}}\left[\varepsilon_x + \nu_{yx}\varepsilon_y\right] = \frac{E_x h}{1-\nu_{xy}\nu_{yx}}\left[-\frac{w}{R} + \nu_{yx}\varepsilon_y\right] \qquad \{36a\}$$

$$N_y = \frac{E_y h}{1-\nu_{xy}\nu_{yx}}\left[\varepsilon_y + \nu_{xy}\varepsilon_x\right] = \frac{E_y h}{1-\nu_{xy}\nu_{yx}}\left[\varepsilon_y - \nu_{xy}\frac{w}{R}\right] \qquad \{36b\}$$

If expressions {36} are compared and if Maxwell's expression $\frac{\nu_{xy}}{E_x} = \frac{\nu_{yx}}{E_y}$ is employed it can be found that:

$$N_x = E_x\left[\frac{N_y\nu_{yx}}{E_y} - h\frac{w}{R}\right] = N_y\nu_{xy} - E_x h\frac{w}{R} \qquad \{37\}$$

In Figure 15 the membrane forces {37} shown on the strip jk yield a component of force in the z direction, the magnitude of which per unit length is:

$$\frac{N_x}{R} = \frac{1}{R}\left[N_y\nu_{xy} - E_x h\frac{w}{R}\right] \qquad \{38\}$$

Summing all z direction loads per unit length of strip jk yields:

$$\frac{N_y\nu_{xy}}{R} - E_x h\frac{w}{R^2} + N_y\frac{d^2w}{dy^2} \qquad \{39\}$$

where the last term represents the component of transverse load due to the membrane load N_y acting through the out-of-plane deformation *w*. Thus the differential equation for the bending of the strip jk is:

$$D_2\frac{d^4w}{dy^4} = \frac{N_y\nu_{xy}}{R} - E_x h\frac{w}{R^2} + N_y\frac{d^2w}{dy^2} \qquad \{40\}$$

The deformation *w* will be referenced to the middle surface of the cylinder after the uniform compression N_y is applied. Thus w will be replaced by:

$$w \Rightarrow w + \frac{N_y\nu_{xy}R}{E_x h} \qquad \{41\}$$

and the differential equation becomes:

$$D_2\frac{d^4w}{dy^4} - N_y\frac{d^2w}{dy^2} + E_x h\frac{w}{R^2} = 0 \qquad \{42\}$$

The cylindrical shell is expected to buckle into axisymmetric modeshapes that can be represented by the waveform:

$$w = -A\sin\frac{n\pi y}{b} \qquad \{43\}$$

Inserting expression {43} into {42} and eliminating like terms yields:

$$\frac{R^2h^3n^4\pi^4E_y + 12b^2\left(hb^2E_x + R^2n^2\pi^2N_y\right)\left(1-\nu_{xy}\nu_{yx}\right)}{12R^2b^4\left(1-\nu_{xy}\nu_{yx}\right)} = 0 \qquad \{44\}$$

Solving expression {44} for N_y yields:

$$N_y = -\frac{hb^2E_x}{R^2n^2\pi^2} - \frac{h^3n^2\pi^2E_y}{12b^2\left(1-\nu_{xy}\nu_{yx}\right)} \qquad \{45\}$$

Thus an expression has been produced that relates the axial load per unit length to the half wave number *n*. The goal is to determine the minimum value of N_y associated with any buckled shape. A new variable λ is substituted for $n\pi/b$ in expression {45}:

$$N_y = -\frac{hE_x}{R^2\lambda^2} - \frac{h^3\lambda^2E_y}{12\left(1-\nu_{xy}\nu_{yx}\right)} \qquad \{46\}$$

In the interest of developing a closed form solution for the critical buckling stress it will be assumed that λ is a continuous variable. The value of λ which will be associated with the minimum value of the membrane force N_y, which is just sufficient to induce instability, is found by equating the derivative of expression {46} with respect to λ equal to zero.

$$\frac{\partial N_y}{\partial \lambda} = \frac{2hE_x}{R^2\lambda^3} - \frac{h^3\lambda E_y}{6\left(1-\nu_{xy}\nu_{yx}\right)} = 0 \qquad \{47\}$$

There are four roots to this equation, only one of which is real and positive:

$$\lambda = \frac{n\pi}{b} = \sqrt{\frac{2}{Rh}}\sqrt[4]{\frac{3E_x\left(1-\nu_{xy}\nu_{yx}\right)}{E_y}} \qquad \{48\}$$

Substituting this root back into expression {46} yields the critical buckling load:

$$N_{ycr} = -\frac{h^2}{R}\sqrt{\frac{E_xE_y}{3\left(1-\nu_{xy}\nu_{yx}\right)}} \qquad \{49\}$$

Thus the critical stress required to buckle a sector of an orthotropic cylinder is:

$$\sigma_{ycr} = -\frac{h}{R}\sqrt{\frac{E_xE_y}{3\left(1-\nu_{xy}\nu_{yx}\right)}} \qquad \{50\}$$

where the associated half wave number *n* can be found using expression {48}. This number should be truncated to an integer in keeping with the definition of the half wave number. Also note for isotropic conditions that expression {50} simplifies to expression {35}. At the beginning of this section it was noted that the σ_y stress required to wrinkle a web was much larger than that required to trough a web. To form an estimate of this expression {35} can be divided by expression {6} to yield:

$$\frac{\sigma_{ycr,wrinkle}}{\sigma_{ycr,trough}} = \frac{\dfrac{Eh}{R\sqrt{3\left(1-\nu^2\right)}}}{\dfrac{\pi h}{a}\sqrt{\dfrac{E\sigma_x}{3\left(1-\nu^2\right)}}} = \frac{a}{\pi R}\sqrt{\frac{E}{\sigma_x}} \qquad \{51\}$$

Substituting common values for span length a, roller radius R, web modulus E, and the stress due to web tension σ_x it can be found that the σ_y stresses required to wrinkle a web can easily be 100 to 200 times greater than the σ_y stresses required to induce troughs in the web. What is the source of these larger σ_y stresses required to induce wrinkles? This will be the topic of the next section.

TENSION FIELD BUCKLING

The first calculations of tension field buckling were made for thin webs of aluminum used in aircraft structure [7]. These thin webs buckle or trough at low shear levels but the webs are surrounded by axial stiffeners which are various extruded shapes. After buckling the web can accept much higher shear levels because these shears develop tensile stresses in the direction of the troughs or buckles that are reacted by compressive stresses in the axial stiffeners that surround the panel. In the case of a web traveling through process machinery the axial stiffeners are the shells of web that form when the web wraps a roller. As shown in Figure 1 each free span of web is bounded at their upstream and downstream edges by a web shell stiffener but there are also two edges which are free.

After web troughs precipitate per expressions {6} or {17} some form of post buckling analysis must be employed to study how the free spans with troughs induce compressive stresses in the web shells. For thin webs the value of the flat web buckling stress predicted by expressions {6} or {17} is both small from an absolute sense and small relative to the shell buckling stress predicted by expressions {35} or {50}. In tension field theory it is assumed that no compressive stress can be reacted by a web panel.

A method which was proposed by Miller and Hedgepeth [8] has been adapted in commercial finite element codes. Their method is based upon altering the constitutive relations between stress and strain for two dimensional finite elements:

$$\begin{Bmatrix} \sigma_x \\ \sigma_y \\ \tau_{xy} \end{Bmatrix} = [D] \begin{Bmatrix} \varepsilon_x \\ \varepsilon_y \\ \gamma_{xy} \end{Bmatrix} \qquad \{52\}$$

There are three potential stress states in tension field behavior. In one of these states, the element is taut which means that both principal stresses are larger than zero. In this case the [D] matrix is that which is associated with plane stress:

$$D_{taut} = \frac{E}{1-\nu^2}\begin{bmatrix} 1 & \nu & 0 \\ \nu & 1 & 0 \\ 0 & 0 & (1-\nu)/2 \end{bmatrix} \quad \text{used when } \varepsilon_1 > 0 \text{ and } \nu > -\frac{\varepsilon_2}{\varepsilon_1} \qquad \{53\}$$

The second state is one in which a particular finite element has buckled and it is assumed the second principal stress σ_2 is zero. A new [D] matrix is employed of the form:

$$D_{buckled} = \frac{E}{4}\begin{bmatrix} 2(1+P) & 0 & Q \\ 0 & 2(1-P) & Q \\ Q & Q & 1 \end{bmatrix} \quad \text{used when } \varepsilon_1 > 0 \text{ and } \nu < -\frac{\varepsilon_2}{\varepsilon_1} \qquad \{54\}$$

$$P = \frac{\varepsilon_x - \varepsilon_y}{\varepsilon_1 - \varepsilon_2} \text{ and } Q = \frac{\gamma_{xy}}{\varepsilon_1 - \varepsilon_2}$$

The final state is one in which an element has gone completely slack and thus both principal stresses are zero (σ_1=σ_2=0). Now a [D] matrix is employed of the form:

$$D_{slack} = \begin{bmatrix} 0 & 0 & 0 \\ 0 & 0 & 0 \\ 0 & 0 & 0 \end{bmatrix} \quad \text{used when } \varepsilon_1 < 0 \qquad \{55\}$$

Use of these constitutive relations requires iterative analysis. Loads are applied in several load steps. During the first load step taut behavior is initially assumed in all elements followed by computations of Cartesian strains and principal strains within each element. Then the principal strains are reviewed using the strain criterion specified in expressions {53,54,55} to determine which behavior (taut, wrinkled, or slack) should have existed in that element. In a second iteration computations would be carried out using the [D] matrix which was appropriate for that element. Further iteration is needed because the [$D_{buckled}$] matrix is dependent on strains that were computed in a previous solution. Thus iteration must be performed until some level of convergence in P and Q is attained. After convergence is obtained for one load step the computations proceed to a next load step which now can begin with an initial state with the [D] matrices for all elements that were converged in the previous load steps. As loads increase elements that were previously taut may become wrinkled and those that were wrinkled could become slack and thus the principal strain criteria in expressions {53-55} must be continually reviewed for each element. Again for wrinkled elements, iterative solutions are required until convergence in P and Q in expression {54} are obtained.

Prediction of Wrinkles due to Misaligned Rollers

Experiments on webs in spans where a downstream roller is initially aligned and then slow misaligned always follow a pattern. Initially the web is flat and remains so until the critical misalignment to induce troughs is attained. Further misalignment will result in the troughs becoming deeper and reducing the projected width of the web mid-span between rollers. Yet further misalignment will finally induce wrinkles in the shells of web material on the rollers. To capture the behavior from trough formation to the onset of wrinkling finite element models were developed using the tension field elements described previously. In these models the web in the entering free spans would be modeled with the wrinkle membrane elements which can either exhibit taut, wrinkled or slack behaviors depending on the ratio of the principal strains (53-55). The elements representing the shells of web on the rollers were capable only of exhibiting taut elastic behavior. The exiting free span was modeled with taut elastic elements as well. A typical model is shown in Fig. 16.

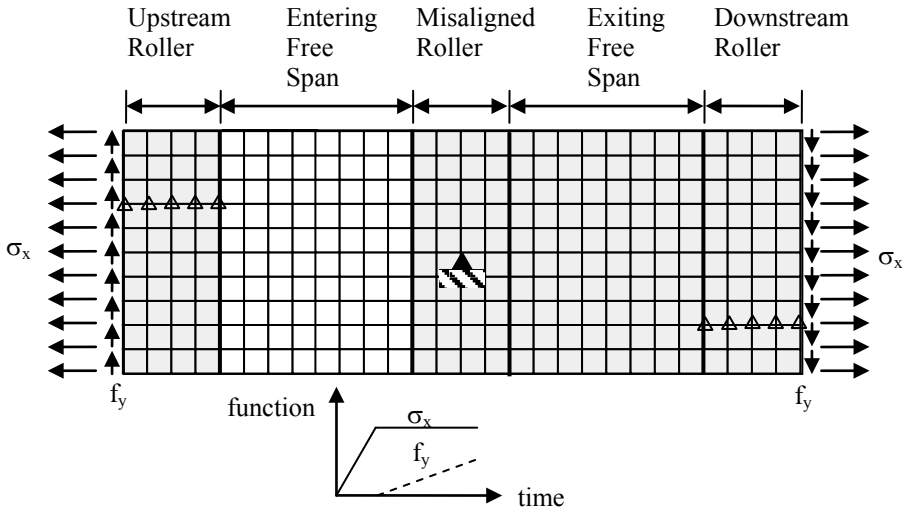

Figure 16 – Typical Finite Element Model used in Roller Misalignment Wrinkling Analysis

To ensure accuracy in the modeling special attention had to be given to constraints and kinetic boundary conditions. The objective of the modeling was to study compressive principal stresses that would develop in the elastic elements used to represent the web on the misaligned roller. A pin constraint was provided at the center of the model as shown. The applied surface tractions σ_x and f_y should cancel one another on the two *x* faces leaving the reactions at the pinned node to be zero. Note the mesh is symmetric about a vertical axis of symmetry passing through the pin constraint. This was done to ensure that the *x* direction stress was as uniform as possible in the region of the misaligned roll to sustain Shelton's zero moment kinetic boundary condition at the misaligned roller. Each line of nodes crossing the upstream roller in an *x* direction was given a multipoint constraint which would lock the *y* direction deformations of those nodes together. These multipoint constraints, shown as groups of triangles above, enforce normal entry of the web to a roller but they also allow the Poisson contraction of the web due to the applied tensile stress σ_x in the *x* direction. This type of analysis is nonlinear and thus the loads are incremented in time steps. As shown in the plot in Fig. 16 the level of stress σ_x due to web tension would be raised to a desired level in the first few load steps.

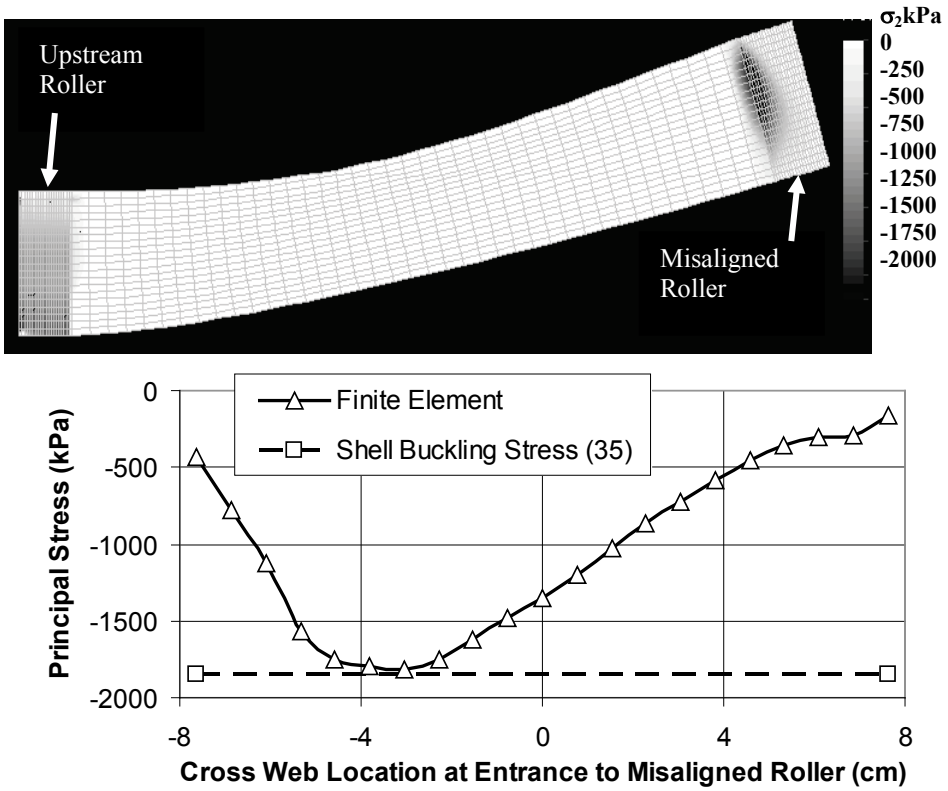

Figure 17 – Model Results

Then the f_y loads would be raised from zero to a test value. After executing the model the compressive principal stresses in the elastic elements on the misaligned roller were reviewed. If those stresses were less than the classic shell buckling stress given by expression (35), a factor which multiplied the f_y forces would be increased and the finite element computations would be conducted again. Whenever the compressive principal stress in the elements on the roller became essentially equal to the predicted buckling stress (35)

the computations would cease. The lateral deformations of the nodes in the web on the misaligned roller would then be used to estimate $\theta_{critical}$, the misalignment of the roller required to induce wrinkling in the web on that roller.

The results of such modeling are shown in Fig. 17 for a polyester web 15.24 cm (6 in) wide with a free entering span 76.2 cm (30 in) long. The web thickness and material properties were identical to that mentioned earlier for the trough tests. The roller diameter was 7.37 cm (2.9 in). In this example the web was subject to a tension of 73.7 N (16.56 lb). A contour map of the second principal stresses is shown for the web on the upstream roller, the entering span and the web on the misaligned roller. Note the pocket of compressive stress that has formed in the elastic elements at the entry to the misaligned roller. To quantify these stresses a chart has also been in included in Fig. 17. In this case the shell buckling stress per expression (35) is -1.92 MPa (-278 psi). The f_y forces were

increased until the minimum principal stress and the shell buckling stress were equal as shown in Fig. 17. At this level of tension and lateral force the misalignment θ_j was found to be 0.0245 radians. With a model created for a given entry span of length *a* the analysis was repeated for various web tension levels.

Using the same experimental apparatus described in Fig. 5 several wrinkle experiments were conducted on the web described above. Two additional models were meshed similar in all aspects to the model described above except that the entry span length was shortened to 15.24 cm (6 in) and 45.7 cm (18 in). Analyses and tests were conducted at multiple web tension levels.

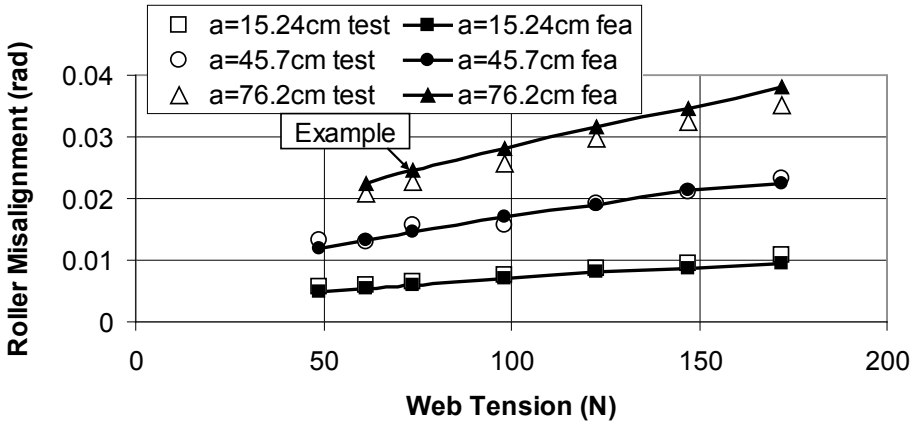

Figure 18 – Comparison of Wrinkling Predictions with Test Results on 23.4 □m Polyester Film

The results are shown in Fig. 18 with the agreement between experimental tests and the finite element method being acceptable. Note that the calculations shown in Fig. 17 and the supporting text are shown as the "Example" calculation in this figure.

Prediction of Wrinkles due to Tapered Rollers

The analysis is similar to that of the misaligned rollers but now the boundary conditions for the tapered roller are enforced as shown in Figure 19. Again the elements with a white background are the elements that can assume the wrinkle membrane behavior and the elements in gray are elements that can assume only elastic behavior. A notable difference from the misaligned roller model is the additional sets of lateral forces. This arrangement imposes constant moment in the web between the entry and the exit of the tapered roller. The coupling constraints are used again to enforce normal entry and exit to the upstream and downstream rollers. They are also used at the entry to the tapered roller as shown to enforce normal entry to the tapered roller as well.

In these analyses the machine direction stress was brought to a fixed level in a few load steps and then the lateral forces f_y would be slowly increased until the second principal stress became equal to the critical shell buckling stress from expression (35). An example will be given for a 23.4 μm polyester web with a span length of 76.2 cm (30 in) and a web width of 15.24 cm (6 in). In this example the web tension was increased to 58.9 N which exerted a uniform stress of 16.5 MPa on the web. The lateral forces were then increased until the second principal stress equaled the buckling stress as shown in Figure 20. In this case the shell buckling stress per expression (35) is -1.92 MPa (-278

psi) for a polyester web with the properties shown in Table 1 passing over rollers whose nominal radii were 3.68 cm (1.45 in). The machine or x direction stresses have become non-uniform as a result of the lateral forces and are shown in Figure 21. These stresses can be integrated over the width of the web using expression (30) to obtain the moment M_j, about 104.1 N-cm in this case. Then using expression (30) again the equivalent roller taper *m* that would have induced this moment can be found, about 0.00113 cm/cm in this example.

Using the experimental apparatus shown earlier in Figure 11 wrinkle test data was collected using a 23.4 μm polyester web which was 15.24 cm wide. The wrinkle test data and the finite element model results have been superimposed on the earlier trough test data and the closed form algorithm for troughs given by expression (34) in Figures 22, 23, and 24 for span lengths of 50.8, 76.2, and 101.6 cm. In total the agreement is quite good. The example case is shown Figure 23.

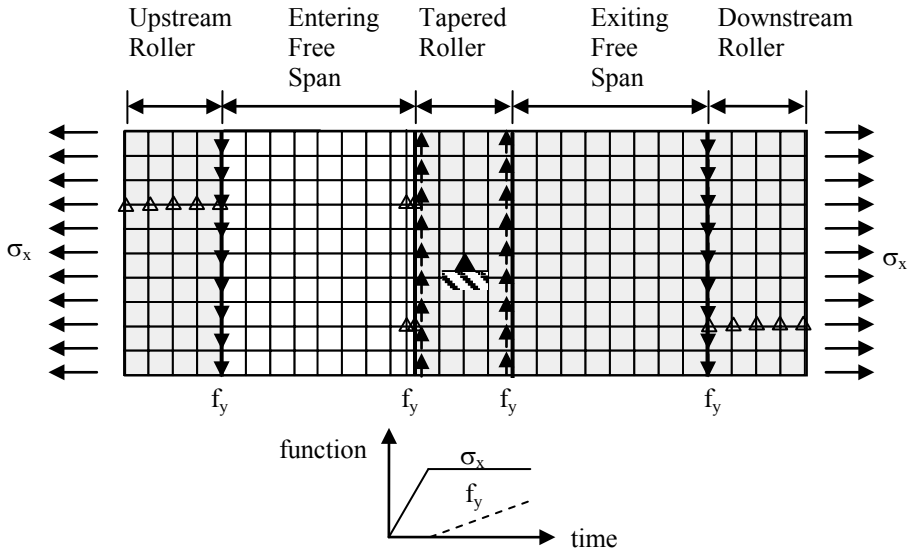

Figure 19 – Finite Element Model of a Web Encountering a Tapered Roller

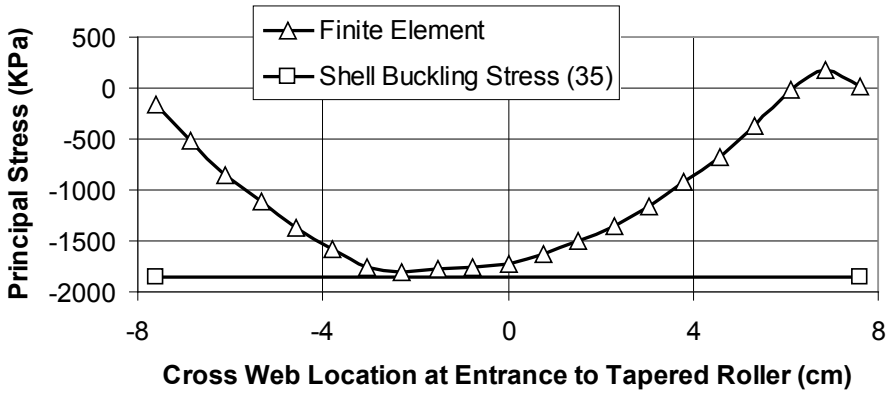

Figure 20 – Second Principal Stress in Web at Entry to the Tapered Roller for a Span Length of 76.2 cm and a Web Tension of 58.9 N

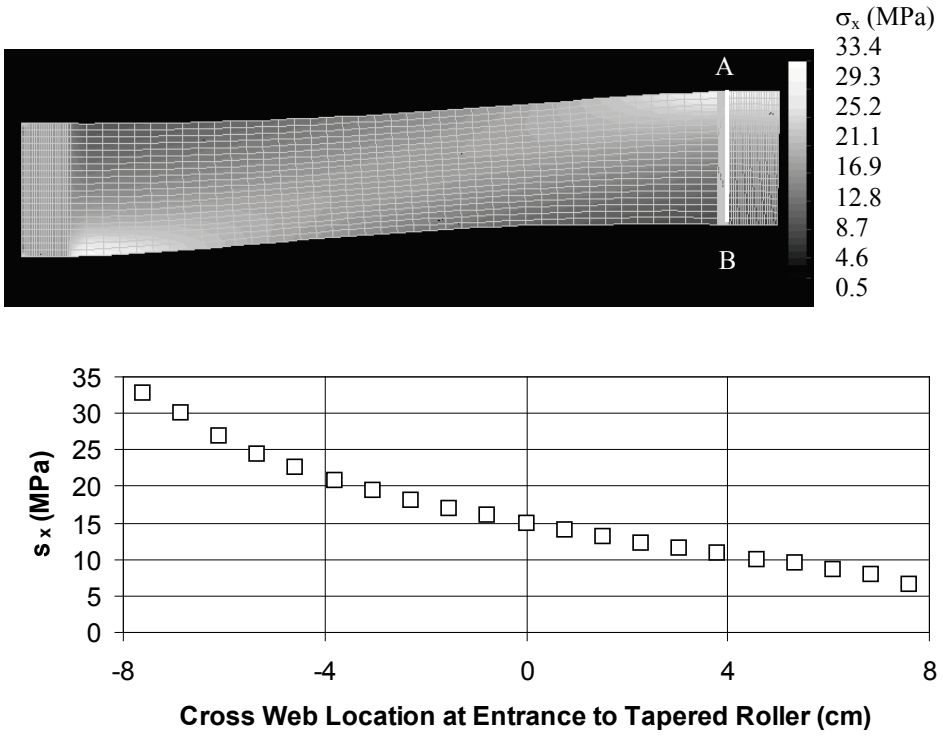

Figure 21 – Machine Direction Web Stress as the Web Contacts the Tapered Roller (Line A-B) for a Span Length of 76.2 cm and a Web Tension of 58.9 N

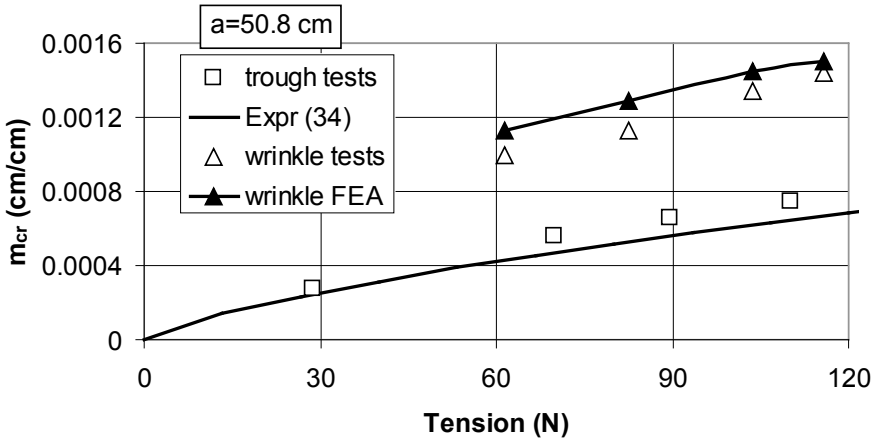

Figure 22 – Troughs and Wrinkles in a 23.4 mm Polyester Web in a Web Span of 50.8 cm

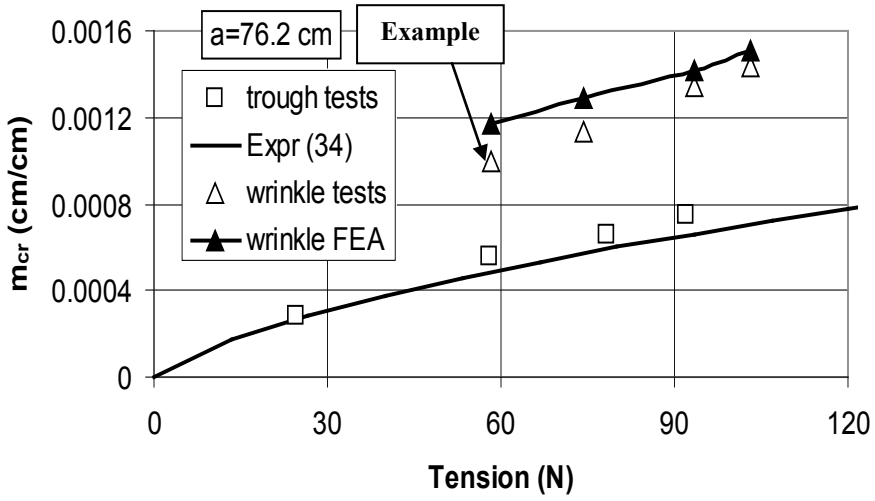

Figure 23 – Troughs and Wrinkles in a 23.4 mm Polyester Web in a Web Span of 76.2 cm

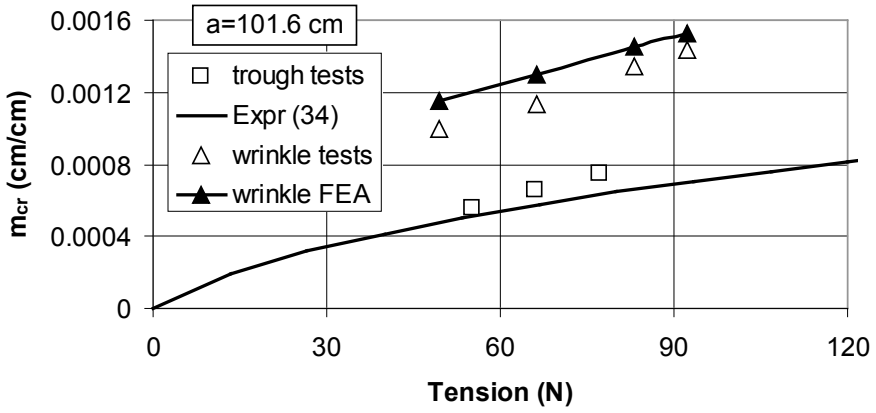

Figure 24 – Troughs and Wrinkles in a 23.4 mm Polyester Web in a Web Span of 101.6 cm

Prediction of Wrinkles due to Holes in Webs

Perhaps producers of paper would wonder why one would want to transport a web with holes in it, perhaps converters of webs would wonder why not? Converting operations often require shapes to be cut in webs and then the web must be handled in process machines, preferably without wrinkles. Often wrinkles form due to web non-uniformities rather than roller alignment or taper problems that have been previously examined. In this case the propensity of a web with a centrally located hole to wrinkle will be studied. The problem was first studied in the laboratory. A hole of diameter 1.27 cm (1/2 in) was bored centrally in a roll of 20.1 μm (0.00079 in) thick polyester film with a width of 30.5 cm (12 in). The roll was unwound and the web was transported through a test section in a span of 71.1 cm (28 in) long over rollers with a radius of 5.08 cm (2 in). One observation was that the hole did cause troughs to form about the hole and wrinkles to form on the downstream roller. The troughs extended upstream and downstream from the hole as seen in Figure 25. As the hole neared the downstream roller two troughs on either side of the hole would form a wrinkle on the surface of the downstream roller. A second observation was that the level of web tension affected the distance between the hole and the downstream roller when the wrinkles would first appear on the downstream roller.

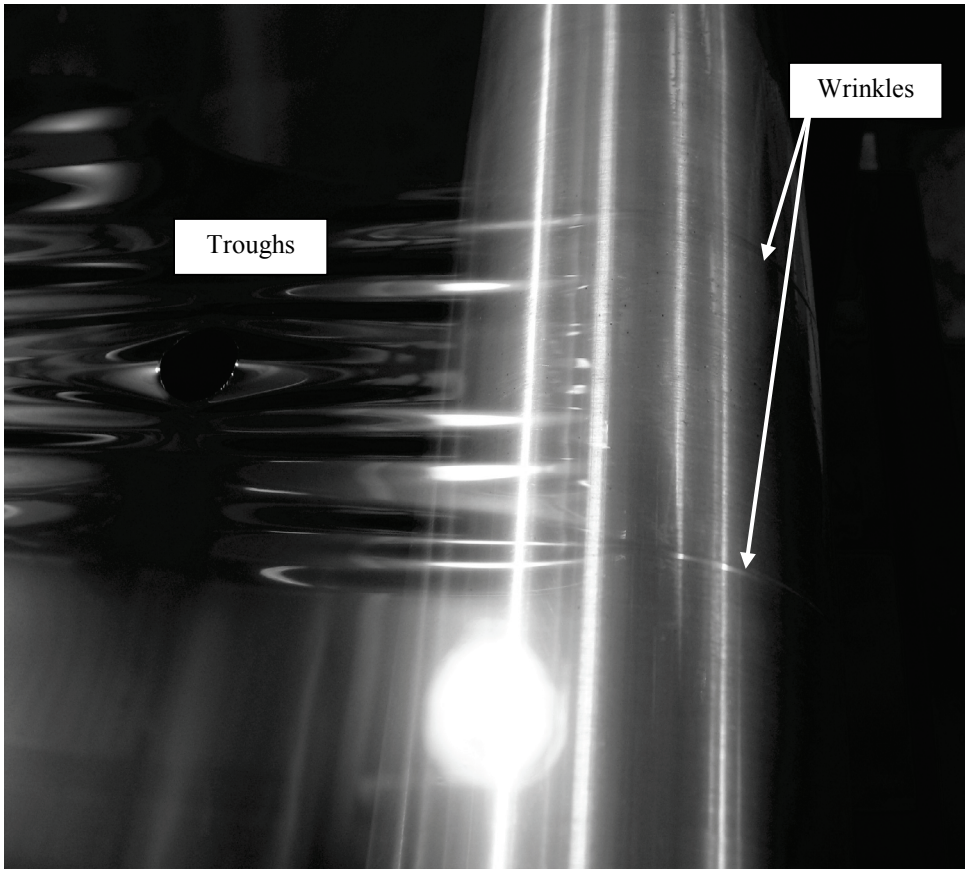

Figure 25 – Troughs and Wrinkles due to a Circular Void in the Web

At low values of web tension the hole had to travel close to the downstream roller before wrinkles appeared and if low enough they might not appear at all. At high values of web tension the distance between the hole and the downstream roller was much larger when wrinkles formed on the downstream roller. Typically two wrinkles would form, one on either side of the hole as shown in Figure 25.

Data collection then began. At fixed values of web tension the machine direction distance between the hole and the point of contact of the web with the downstream roller was recorded when a wrinkle formed. Also the distance between the two wrinkle initiation points on the roller was recorded. The distances L and W that were recorded are perhaps made clearer in Figure 26.

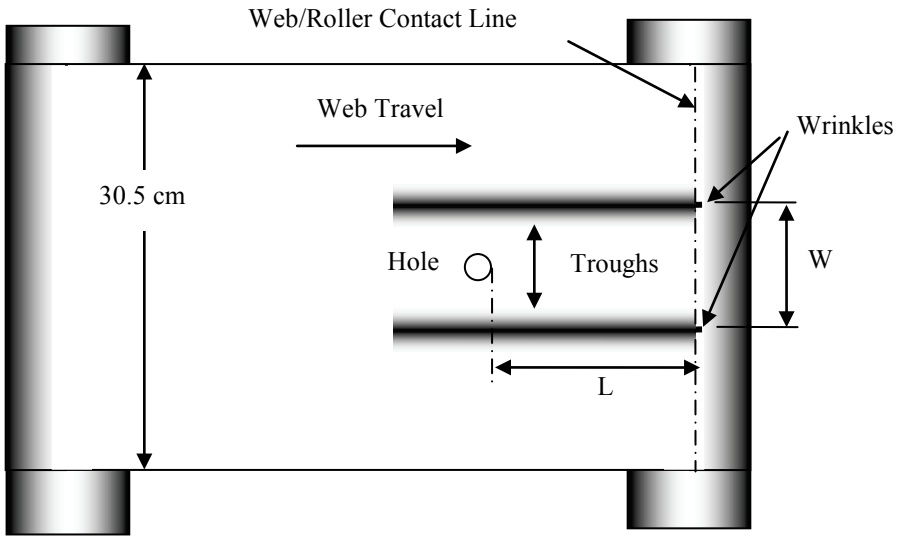

Figure 26 – Distances recorded at the Onset of Wrinkling

Nonlinear finite element analyses of the type described earlier for wrinkles due to roller misalignment and to roller taper were conducted. Higher order elements were used in this analysis which allowed the modeling of the hole boundaries with precision. In Figure 27 a schematic of the finite element model is shown. Note that the center line of the web was prevented from deforming in the cross machine direction. In these analyses the σ_x machine direction stress was increased linearly until negative cross machine direction stresses of the amplitude of the critical shell buckling stress (35) was attained.

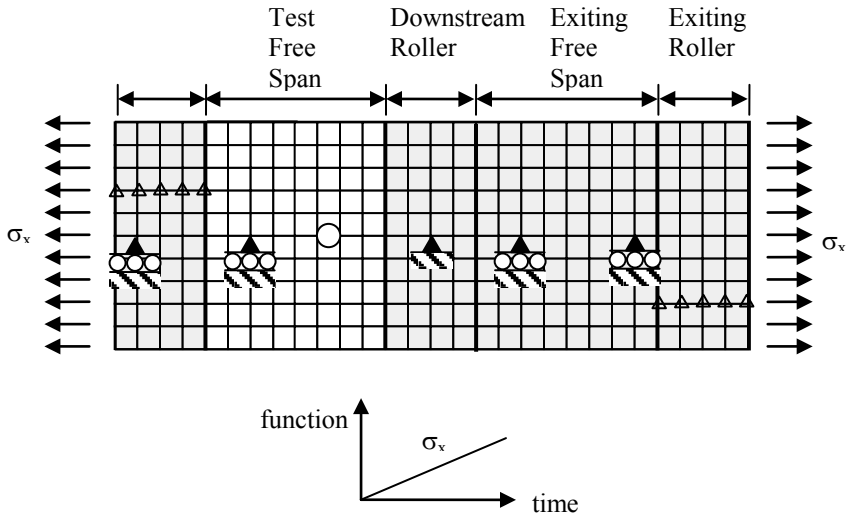

Figure 27 – Schematic of Finite Element Model

A plot of the second principal stresses can be seen in Figure 28. The case being modeled is the experimental test case described earlier. In this instance the downstream edge of the 3.68 cm (1/2 in) hole is 10.2 cm (4.0 in) from the contact line between the web and the downstream roller. The contact line is denoted by the line A-B in the stress plot. Note the chart of these stresses as well in the figure. This polyester had a Young's modulus of 4892 MPa (710,000 psi), Poisson's ratio was assumed to be 0.3 and for the web thickness and roller radius of these tests the shell buckling stress was found to be -1,170 KPa (-170 psi) using expression (35). Note the finite element solution shows the principal stress becomes minimum and equal to the shell buckling in two locations which border the hole when the applied MD σ_x level in Figure 27 was 32.1 MPa (4660 psi).

Finally in Figure 29 a comparison of the experimental test results and the finite element results are shown. The agreement is quite good especially on the comparison of the *L* dimension. The agreement on the *W* dimension is good and could have been improved further by increasing the finite element mesh density. Note the example case presented in Figure 28 is tagged as *Example* in the finite element data presented in Figure 29.

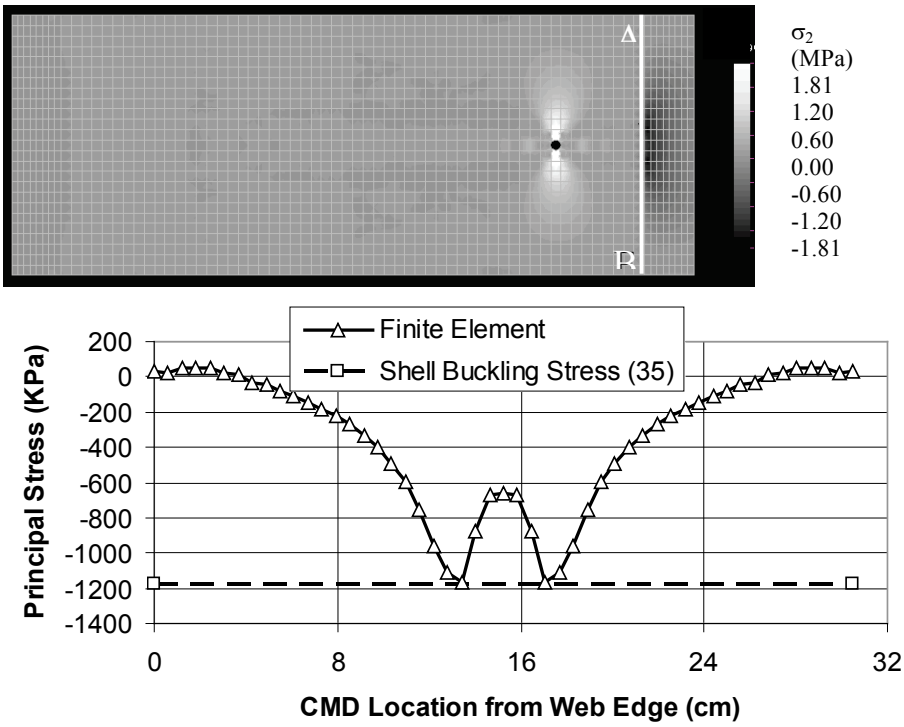

Figure 28 – Finite Element Output of the Principal Stress with a Chart of those Stresses on Line A-B at an applied σ_x Stress Level of 32.1 MPa

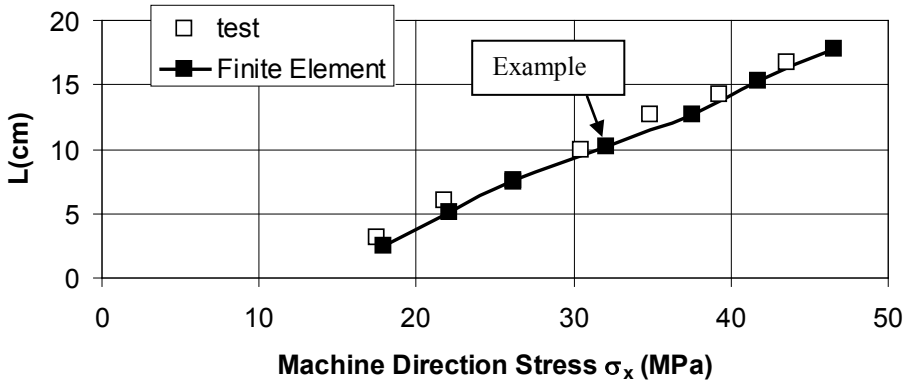

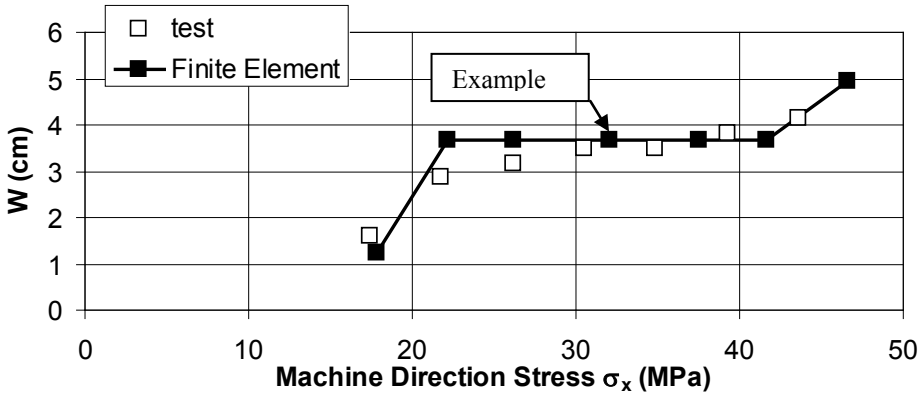

Figure 29 – Test Results and Finite Element Prediction of the Proximity of the Hole to the Downstream Roller at Wrinkle Formation (L) and the Distance between Wrinkles (W)

CONCLUSIONS

Three examples have been presented where it was shown that the existence of troughs in web spans were a necessary precursor to web wrinkles being formed on rollers. For the case of the web approaching a misaligned or tapered roller closed form expressions were developed to predict the occurrence of troughs. Nonlinear finite element analysis using membrane tension field elements were used to study the compressive CMD principal stresses that form as the web contacts a roller after the web in the free spans has troughed. No closed form expression for troughs due to holes in webs was presented and may not exist but in fact this could be studied using linear finite analysis and elastic elements. Whenever the second principal stress becomes more negative than that given by expressions {6} and {17}, troughs could be forecast. Regardless of the source of the troughs once they appear negative CMD second principal stresses will be created in the web as it enters the downstream roller. These negative principal stresses will become more negative if whatever the source that produced the troughs to begin with becomes larger. In the case of the misaligned roller the critical misalignment given by expressions {6} or {17} was required just to make troughs appear. At that point the negative CMD principal stresses in the web on the downstream roller were small. Additional roller misalignment was required to produce CMD principal stresses that were more negative than the shell buckling stress given by expressions {35} if the web is isotropic or {50} if it be orthotropic. At that amount of misalignment web wrinkles will occur. Similarly it was found that a certain amount of roller taper was required to produce a trough but a much higher level was required to produce a wrinkle. In the final case it was difficult to find conditions where a hole in the web would not result in troughs but the hole and the troughs that surrounded it had to be within a certain distance within the downstream roller to produce a wrinkle. In this case the hole and the web tension act together to create the disturbance and higher values of web tension will be able to create wrinkles with the hole further away from the downstream roller. If the web tension was low enough the hole could either get quite close to the downstream roller before wrinkles were created and yet lower web tensions resulted in no wrinkles forming. Conclusions that can be drawn from these analyses include:

- Troughs can be predicted in free spans given means for predicting the compressive σ_y stresses due to a disturbance and the critical buckling stresses given in expressions {6} and {17}.
- The nonlinear finite element analyses using the Miller-Hedgepeth wrinkle membrane elements enable the accurate calculation of the negative CMD principal stresses in the web at the entry to the downstream roller.
- The shell buckling criteria given in expressions {35} and {50} are accurate predictors for wrinkles.

Perhaps the greatest contribution of this work is that it presents a systematic method for studying the formation of troughs and wrinkles in webs. Troughs form for many reasons in webs. The examples presented herein are based on machine or web imperfections. It is common in web process machinery to locally add moisture or to locally increase temperature both of which can result in trough formation [9]. Once it is understood that wrinkle formation is dependent on trough formation one can seek to eliminate the source of troughs to eliminate wrinkles.

ACKNOWLEDGEMENTS

The authors would like to thank the industrial sponsors of the Web Handling Research Center at Oklahoma State University for providing the resources which made this research possible.

REFERENCES

1. Timoshenko, S. P. and Gere, J. M., Theory of Elastic Stability, 2nd ed., McGraw-Hill, New York, 1961, pp. 348-359.
2. Lekhnitskii, S.G., Anisotropic Plates, 2nd ed., Gordon and Breach, New York, 1968, p. 456.
3. Shelton, J. J. and Reid, K. N., "Lateral Dynamics of a Real Moving Web," ASME Journal of Dynamic Systems, Measurement, and Control, Vol. 93, No. 3, 1971, pp. 180-186.
4. Przemieniecki, J. S., Theory of Matrix Structural Analysis, McGraw-Hill, New York, 1968, pp.70-80, 388-391.
5. Timoshenko, S. P. and Gere, J. M., Theory of Elastic Stability, 2nd ed., McGraw-Hill, New York, 1961, pp. 457-460, 485-486.
6. Weingarten, V. I., Morgan, E. J., and Seide, P., "Elastic Stability of Thin-Walled Cylindrical and Conical Shells under Combined Internal Pressure and Axial Compression," AIAA Journal, Vol. 3, No. 6, 1965, pp. 1118-1125.
7. Kuhn, P., Peterson, J.P., and Levin, L.R., "A Summary of Diagonal Tension: Part 1 Methods of Analysis," NACA Tech. Note 2661,1952.
8. Miller, R. K. and Hedgepeth, J. M., "An Algorithm for Finite Element Analysis of Partly Wrinkled Membranes," AIAA Journal, December, 1983, pp. 1761-1763.
9. Kulachenko, A., Gradin, P., and Uesaka, T., "Tension Wrinkling and Fluting in Heatset Web Offset Printing Process – Post-Buckling Analyses," Advances in Paper Science and Technology, Transactions of the 13th Fundamental Research Symposium, Cambridge, UK, Sept. 2005, pp. 1075-1100.

Keynote Presentation – *Predicting Web Wrinkles on Rollers*	**J. Beisel, H. Yurtcu & J. K. Good,** Oklahoma State University, USA

Name & Affiliation	**Question**
	No Questions until Discussion